Cell Biochem Biophys (2018) 76:231–241
DOI 10.1007/s12013-017-0830-5

ORIGINAL PAPER

Cysteine to Serine Conversion at 111th Position Renders the Disaggregation and Retains the Stabilization of Detrimental SOD1 A4V Mutant Against Amyotrophic Lateral Sclerosis in Human—A Discrete Molecular Dynamics Study

E. Srinivasan[1] · **R. Rajasekaran**[1]

Received: 17 June 2017 / Accepted: 18 September 2017 / Published online: 26 September 2017

Abstract Protein aggregation is a hallmark of various neurodegenerative disorders, such as amyotrophic lateral sclerosis (ALS) in humans. Mutations in Cu/Zn superoxide dismutase (SOD1) protein were found to be a prominent cause behind the majority of the familial ALS cases with abnormal protein aggregates. Herein, we report the biophysical characterization of the beneficial mutation C111S that stabilizes the SOD1 harboring A4V mutation, one of the most lethal diseases causing mutant that leads to protein destabilization and aggregation. In this study, we utilized discrete molecular dynamics (DMD) simulations, which stipulated an outlook over the systematic action of C111S mutation in the A4V mutant that stabilizes the protein and impedes the formation of protein aggregation. Herewith, the findings from our study manifested that the mutation of C111S in SOD1 could aid in regaining the protein structural conformations that protect against the formation of toxic aggregates, thereby hindering the disease pathogenicity subtly. Hence, our study provides a feasible pharmaceutical strategy in developing the treatment for incurable ALS affecting the mankind.

Keywords ALS · Stabilizing mutant · SOD1 · DMD · Aggregation

Electronic supplementary material The online version of this article (https://doi.org/10.1007/s12013-017-0830-5) contains supplementary material, which is available to authorized users.

✉ R. Rajasekaran
rrajasekaran@vit.ac.in

[1] Department of Biotechnology, School of Bio Sciences and Technology, Bioinformatics Lab, VIT University, Vellore, Tamil Nadu 632014, India

Introduction

Neurodegenerative disorders are progressively widespread among the mankind and exemplify a very noteworthy challenge towards the medical treatments. Various clarifications have been proposed for the origin of the disease, which includes protein aggregation, misfolding, dysfunction, and paralysis. The most important key feature among the neurodegeneration is the protein aggregation, that in turn aids in various pathological events leading to increased cytotoxicity in humans [1–4].

Amyotrophic lateral sclerosis (ALS) is one such neurodegenerative disorder characterized by the degeneration of upper and lower motor neurons that eventually progress towards muscle paralysis and death within 3–5 years of early diagnosis [5–8]. Currently, there is no effective treatment against ALS other than rizoule, which could prolong the survival for 2–3 months [9, 10]. As in ALS, only 10% of the disease onsets remain familial, while the other 90% are sporadic that is widely spread among the human community. Numerous reports indicated that mutations in gene coding Cu/Zn superoxide dismutase (SOD1) are frequent cause for familial and sporadic ALS [11–13]. SOD1 protein functions as a free radical scavenger in the human body that catalyzes the dismutation of the superoxide radicals into hydrogen peroxide and dioxygen. Thus, the mutations in SOD1 hinder the dismutase activity that results towards the toxic gain function of the unfolded protein [14]. Recent studies reported that abnormal non-native SOD1 trimer also exhibit toxicity in cultured cells [15]. So far, the mechanistic action behind the toxic gain of mutant SOD1 remains unclear [16, 17].

Structurally, SOD1 is a homodimeric metalloproteinase enzyme that consists of 153 polypeptides forming eight antiparallel Greek key beta-strands with unique Cu (H46,

48, 63, and 120) and Zn (H63, 71, 80, and D83) ions bounded in each monomer [18–20]. The coordination of Cu and Zn ions is vital for the dismutase activity and the structural stability of SOD1, respectively [21]. The presence of disulfide bond (C57–C146) in SOD1 also aids in retaining the protein stability [22]. In spite of the two-cysteine residues forming the disulfide bond, SOD1 also has two other free cysteine residues C6 and C111 located in the buried and the surface regions, respectively. The sulfur atoms present in cysteine residues are generally attacked by the oxidants and reductants making them relatively vulnerable to oxidative modification. Further, the sulfhydryl moiety present in C111 reacts with the redox substrates, like glutathione or peroxides, thereby forming S–S or S–O covalent modifications, respectively [23–26]. Furthermore, reports from various studies have shown that peroxidase form of C111 moieties is seen in the aggregated form of mutant SOD1. Thus suggesting that C111 act as a principal target for the oxidative modifications in SOD1 [27]. Numerous experimental studies have also suggested that the formation of the protein aggregates were found reduced upon substituting Ser at C111 of different SOD1 mutant forms. Moreover, the disease pathogenicity of the motor paralysis was also seen hindered upon the substitution of C111S in mutant SOD1 [28, 29]. Recently, the phosphomimetic mutation, T2D of SOD1 was identified to thermodynamically stabilize the SOD1 mutant A4V, which is one of the most aggressive ALS-associated mutations in North America. Moreover, the phosphomimetic mutation not only stabilizes but also protects against the formation of toxic SOD1 oligomers [30].

In this study, we utilized computational approaches to shed lights onto the mechanism behind the effect of C111S mutation in reducing the protein aggregation formed by the mutant SOD1. Initially, we studied the most lethal missense disease-causing mutant A4V, which is characterized by the destabilization and formation of toxic aggregates in SOD1. Various reports from the clinical studies have suggested that A4V mutant is highly detected in patients suffering from ALS, which increases the disease progression, and eventually leads towards death within 1.5 years of disease onset [31–33]. To overcome the mutational effect, we reviewed the inhibition of aggregation formation in A4V mutant through a beneficiary mutation at C111S, which was experimentally determined in distinct mutant SOD1 studies [28]. Thus, we employed atomistic simulation to study the effect of these mutations on SOD1, since atomistic simulations have been extensively used as a direct method for investigating the protein aggregation [34–44]. The atomistic simulations were carried out using discrete molecular dynamics (DMD) comparatively for the WT and two other mutant forms, namely, A4V and A4V_C111S. The conformational preferences of the WT and the two other mutant forms were studied in distinct perspective using various geometric tools. In specific, the influence of C111S mutation on protein aggregation was studied profoundly, thus elucidating the mechanistic feature of the mutation on SOD1 in comparison with WT SOD1.

Materials and Methods

Structure Retrieval and Optimization

X-ray crystal structure of monomeric WT and A4V mutant SOD1 was obtained from PDB ID: 2V0A (A) and 1UXM (A) with the resolutions of 1.15 and 1.9 angstroms (Å), respectively [45]. The A4V_C111S mutant was modeled, using Swiss PDB viewer by opting 1UXM structure as a template. The WT and two mutant structures were energy minimized using GROMACS v5.0.4 with GROMOS 43a5 force field [46]. Simple point charge extended water molecules were added. The entire system was solvated within the cubic box with a dimension of 1.0 nm. Addition of a Na^+ ion neutralized the charge of the system. Particle mesh Ewald [47] and Van der Waal's interaction were included. Further, the steepest descent algorithm was employed for performing the energy minimization of WT and MT SOD1 structures with convergence criteria of 5000 steps.

Discrete Molecular Dynamics

Structural dynamics were performed via DMD simulation [48], a distinct molecular dynamics that use a discrete energetic potential for pairwise interaction modeled with the discontinuous functions. Atomistic DMD force field [49] was used in this study. The united atom model was used for the representation of protein model, in which polar hydrogen atoms and heavy atoms were modeled. Bonded interactions comprise of covalent bonds, bond angles, and dihedrals. Non-bonded interactions include van der Waals, solvation, and environment-dependent hydrogen bond interactions [50]. Lazaridis–Karplus implicit solvation model was used for modeling the solvated energy with fully solvated conformations as a reference state [51]. Hydrogen bond interactions were modeled using reaction-like algorithms. Screened charge–charge interactions were modeled, using Debye–Hu¨ckel approximation, by setting Debye length approximately to 10 Å. DMD simulations were performed with constant volume and periodic boundary conditions. Anderson thermostat [52] was used to maintain the constant temperature of 300 K throughout the DMD simulation for WT and two mutant SOD1 forms. Furthermore, the snapshot of WT and mutant SOD1 forms was saved at every 100 time units (tu) throughout the period of

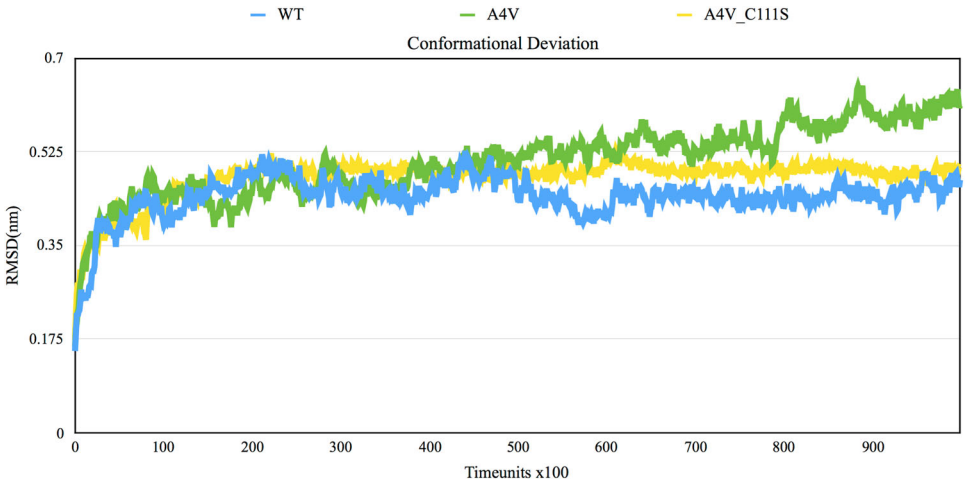

Fig. 1 The conformational stability acquired by the WT and the mutant conformers over the period of simulation time. The SOD1 protein losses the conformational stability upon the A4V mutation as compared to that of WT. The visual representation signifies that the protein conformational stability that was lost due to mutation A4V was found to be regained when S substitutes C111 in the A4V mutant relative to that of the WT

simulation. The tu in DMD simulations refer to the unit of time [*T*] that is determined by units of mass [*M*] with Dalton (1.66×10^{-24} g), length [*L*] with angstrom (10^{-10} m) and energy [*E*] with kcal/mol (6.9×10^{-22} J). Therefore, each time unit corresponds to ~50 fs as of relationship with classical MD [53]. The obtained trajectories were analyzed, using GROMACS programs.

Essential Dynamics

Essential dynamics [54] was performed, using GROMACS to examine the collective motion of WT and mutant SOD1, during the course of simulation. The atomic coordinates obtained from the trajectory were utilized to build the covariance matrix. Hence, the collective motion of WT and two mutants was saved as eigenvectors and eigenvalues that provide the amplitude of their motion. The motion of atoms for each eigenvector displayed the direction of protein motion. Accordingly, the highest amplitude of motions represented in the first two eigenvectors was plotted, to quantify the motion of WT and mutants, throughout the trajectory.

Statistical Calculations

A statistical approach to dynamic analysis provides an influential evaluation with the experimental studies [55]. Thus, the statistical validation of results obtained from the trajectory of WT and mutant SOD1 forms was performed, in this study. In order to statistically verify the variance for the backbone deviation and residual flexibility, non-parametric Wilcoxon rank sum test was performed, using MS Excel. The *P*-value obtained from Wilcoxon method, which provides probability prediction between the WT and two mutant SOD1 forms, signified the outcomes from trajectory analysis.

Result and Discussion

Conformational Stability and Residual Flexibility of WT and Mutant SOD1 Complexes

To endorse the conformational stability of DMD simulations, the root mean square deviation (RMSD) of the backbone Cα atoms from the starting structure of WT and two mutant SOD1 complexes (A4V, A4V_C111S) were computed and plotted as shown in Fig. 1. After the initial tu of simulation, it was observed that WT and A4V_C111S systems were up to equilibration, except for A4V mutant, which lost its conformational stability after 5×10^4 tu. To relate the structural differences, we analyzed the time evolution of the RMSD of backbone Cα atoms averaged for the WT and SOD1 mutants. The average RMSD values of backbone atoms for the WT, A4V, and A4V_C111S were 0.44, 0.50, and 0.47 nm, respectively. Consequently, the substitution mutation of Ala from Val at 4th position of SOD1 had drastically altered the backbone structure as compared to that of WT SOD1 [56–58]. On the other hand, the substitution of S at C111 position in A4V mutant does not impair much change in the backbone structure of SOD1 considerably. Overall, the results from the conformational stability suggested that the A4V_C111S mutation aids in upholding the SOD1 stability near to that of WT when compared with A4V mutant.

In order to study in depth on the aforementioned report, we calculated the residual flexibility of WT and two mutant forms of SOD1 via g_rmsf tool. The residual flexibility characterizes the mobility of a certain residue around its mean position, thereby providing the classified information over dynamical stability of the protein. Figure 2 represents the influence of the two distinct mutations on the flexibility of residues relative to that of WT. In detail, the mutation A4V has radically distorted the overall flexibility of SOD1, most notably, in regions varying from 70–75, 105–110, and

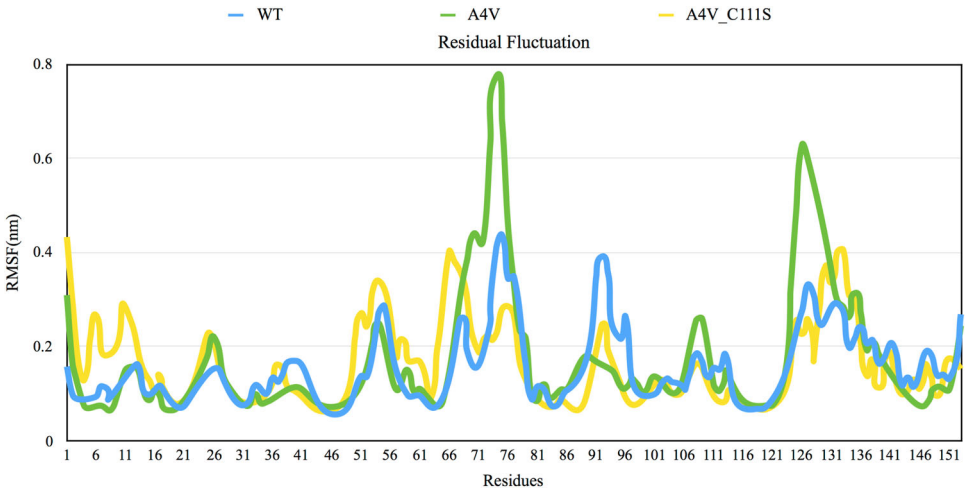

Fig. 2 The conformational flexibility of SOD1 in WT, A4V and A4V_C111S mutant forms over the period of simulation time, indicating the early loss in the residual flexibility upon A4V mutation that were regained when C111 is substituted by S in the A4V mutant

125–130. However, the vice versa was seen upon the insertion of point mutation S at C111 in A4V mutant SOD1. Particularly, the aggregation triggering segments in SOD1 (141–145) that showed lower residual flexibility in A4V mutant was found to retain its flexibility in case of A4V_C111S mutant comparative to that of the WT. Moreover, the computed average residual flexibilities of WT, A4V, and A4V_C111S were also found to be 0.15, 0.17, and 0.16 nm, respectively. Therefore, the results from the residual flexibility correlate with the outcomes of conformational stability indicating that the increased flexibility in A4V mutant had directed towards the loss of protein conformational stability as compared to that of WT and the other mutant form. On the whole, the results from the conformational stability and the residual flexibility altogether endorsed that the point mutation (C111S) on A4V mutant had invariably reduced the protein destabilization and increased flexibility relative to that of WT SOD1. The results from the conformational stability and the flexibility were also statistically analyzed, which showed a significant P-value <0.05. Moreover, the results were further substantiated by preforming multiple replicates that showed similar trend of outcomes for RMSD and root mean square fluctuation values of WT and mutant SOD1 proteins (Supplementary Table 1).

Compactness of WT and the Two Mutant SOD1 Proteins

To understand the overall globularity and folding behavior, the compactness of SOD1 was analyzed via g_gyrate tool. Generally, the overall compactness of a protein corresponds to the protein stability and the intramolecular interactions within a protein structure. In this study, the average values of protein compactness for WT, A4V, and A4V_C111S SOD1 (Fig. 3) were 1.46, 1.49, and 1.47 nm respectively. The value computed for WT SOD1 corresponds with the previously reported value of 1.47 nm [59]. Thus, the results indicated that the A4V mutation had averted the protein folding and the overall compactness of SOD1 as compared to that of WT, whereas the A4V_C111S mutant retained the protein compactness proportional to that of WT. Further, the results indicated that the influence of A4V mutation on SOD1 was neutralized upon substitution of S at C111 in A4V mutant. In addition to above results, the probability distribution of protein compactness in WT and two mutant forms (A4V, A4V_C111S) was plotted (Fig. 4). It was observed that the WT and the A4V_C111S mutant structures have the narrowest distribution of the protein compactness with values varying from 1.45 to 1.50 nm, respectively. The vice-versa trend was observed in A4V mutant structures with the broader distribution of protein compactness values ranging between 1.45 to 1.55 nm. Overall these observations exist in agreement with the above findings, were the A4V mutant protein has less compact structure than that of WT and A4V_C111S proteins. It was suggested that the single point mutation in SOD1 (A4V) has reduced the overall intermolecular interaction and primed SOD1 less stable than WT. Moreover, the substitution of C111 by S in A4V mutant protein possessed greater the intermolecular interaction and more stable structures relative to that of WT. Therefore, the results suggested that the contributing effect of point mutation (C111S) in A4V mutant protein in folded conformation lead to increased structural stability, thus signifying the steady nature of SOD1.

Residual Cross Correlation Map

To provide a better understanding of the residual correlated motions, we computed dynamic cross correlation map for WT and the two mutant forms of SOD1. The cross-correlation matrix element revealed the fluctuations of Cα atoms relative to their average position. The positive and the negative values were represented in blue and yellow colors,

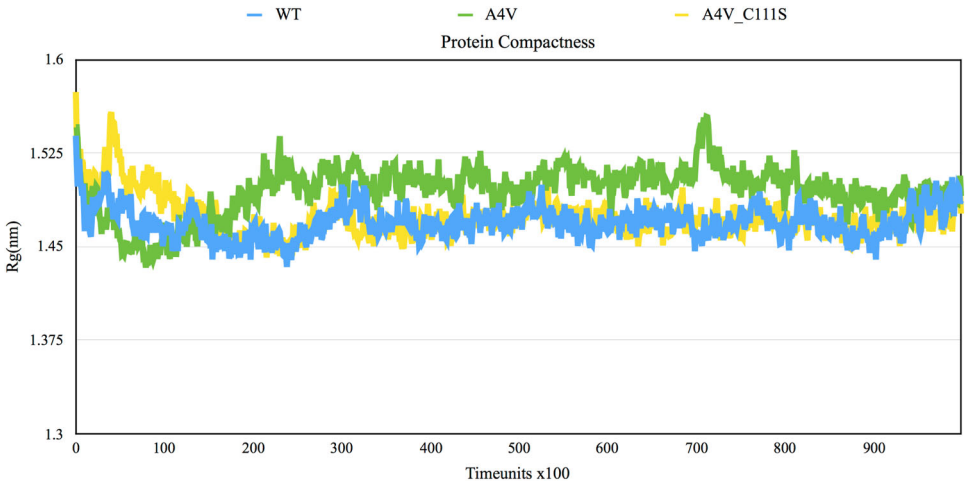

Fig. 3 Protein compactness computed for the WT and the two other mutant forms of SOD1 protein over the dynamic period

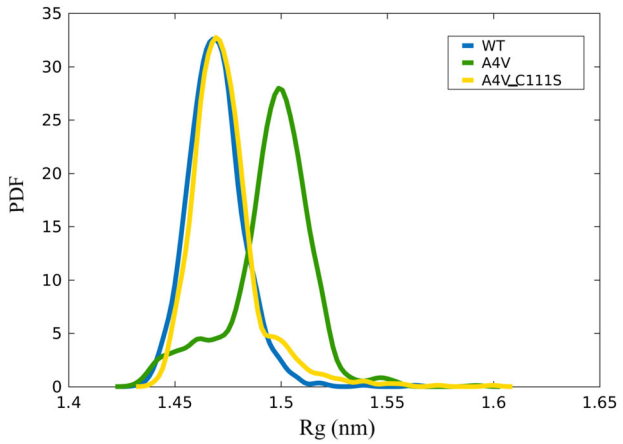

Fig. 4 Probability distribution function of protein compactness for the WT, A4V, and A4V_C111S SOD1 over the entire simulation time

respectively. Positive regions in blue color signified the highly correlated motion in protein, while the negative regions in yellow color defined the strong anti-correlated motion within the protein. From Fig. 5, it was visually observed that the WT have maximum correlated motions between the residues, whereas the vice versa was seen in A4V mutant SOD1. To be noted that the correlated and the anti-correlated motions established within the residues in WT were found less pronounced in SOD1 if V substitutes A4. Moreover, in case of A4V mutant, the substitution of A4 over V had noticeably reduced both the correlated and the anti-correlated motion between the residues that in turn hampered the atomic motion of SOD1 [60]. More interestingly, we found that upon substitution of C111 over S in A4V mutant, the SOD1 regained the correlated motions as compared to that of WT. However, the anti-correlated motions were found reduced in A4V_C111S mutant relative to that of WT. From the above results, It was inferred that the substitution of free C111 by S in A4V mutant could help in retrieving the interatomic protein contacts as that of WT.

Overall, the analyses from the interatomic cross-correlation suggested that the perturbation in the intermolecular interaction of SOD1 upon A4V mutation had critically altered the internal motion and flexibility of protein, which was found to be recovered in A4V_C111S mutant. Hence, the outcomes from dynamic cross-correlation corroborated with the aforesaid analyses indicating the retrieval of SOD1 protein stability, flexibility, interatomic contacts, and compactness in A4V_C111S mutant compared to that of WT.

Essential Dynamics

Subsequently, the significant motion of WT and the two mutant forms (A4V and A4V_C111S) of SOD1 was investigated, using essential dynamics. The first mode of two eigenvectors, which corresponded to principal collective motion, was used to plot the graph of WT and the two mutant forms. The atomic flexibility of WT, A4V, and A4V_C111S was analyzed by the trace of diagonalized covariance matrix, which established their trace values of 13.02, 20.78, and 14.88 nm^2, respectively. Therefore, the analyses suggested that the A4V mutant exhibited increased flexibility in their collective motion as compared to that of WT. However, the reduced flexibility was seen in A4V mutant SOD1, when S substitutes C111. On the basis of the first two largest principal components from ED, the free energy surface was then constructed. The constructed free energy landscape of WT and mutants was represented in Fig. 6 with Gibbs free energy varying from 1 to 10 kcal/mol. The size and shape of the funnel with the globally minimal energy area indicated the stability of a protein. From the projection of two principal components (PCA1 and PCA2) of WT and the two mutants (Fig. 6), it was clear that eigenvectors showed clear difference in collective motion between WT and A4V mutant. On the projections, we observed a cluster of stable states in WT and the vice versa in A4V mutant. In the case of A4V_C111S mutant, the

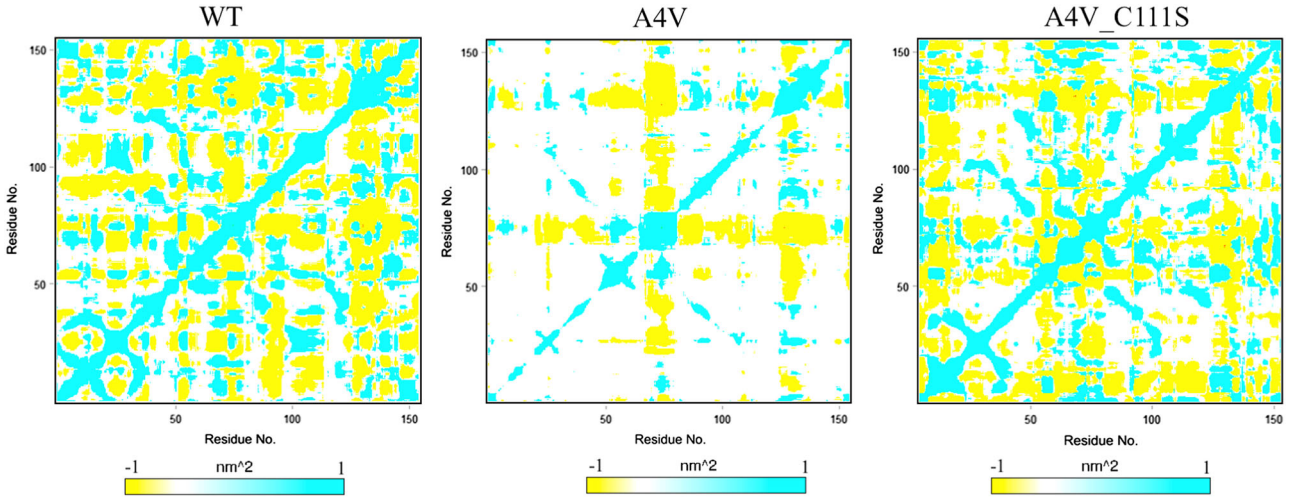

Fig. 5 Dynamic cross-correlation map computed for the WT, A4V, and A4V_C111S SOD1 proteins

projections of PCA1 and PCA2 on the 3-D surface clearly elucidated the cluster of stables that were close to that of WT. Moreover, the global movements of WT SOD1 exhibited a protein folding with a stable global minimum confined within one particular basin (Fig. 6a). Whereas, the point mutation, i.e., A4V on SOD1 had noticeably altered the folding pattern, which led to multiple energy minima acquired by the mutant conformers (Fig. 6b). Therefore, upon substitution of V at A4, the conformational space of SOD1 notably becomes larger and more disperse basins appear on the free energy surface, which suggested that SOD1 no longer have preferred conformations and the initially ordered structure was disturbed by mutation. In contrast, the conformational space acquired by A4V mutant got drastically reduced and were confined within one particular region as that of WT, when S substitutes C111 in A4V mutant SOD1 (Fig. 6c). Thus, the irretrievable changes in the conformational structures of A4V mutant, enriching the pathogenicity of the disease could be reduced upon substitution of C111 by S in A4V mutant SOD1 [28].

Secondary Structural Propensity

In specific, the propensity of alpha helix and beta-sheet exhibit the protein physiological function and the aggregation property [61]. The overall secondary structure propensity was computed for WT and the two other mutant forms, using DSSP tool (Fig. 7). It was signified that the abundance of alpha helix present within the regions of 80–83 and 133–136 in WT (6%) exhibited a major deviation with a reduced propensity of about 1% upon substitution of A4V mutation in SOD1. However, the vice versa (3%) was seen, when the A4V mutant was subjected towards the further substitution S at C111 position. On the other hand, the A4V mutant accelerated the propensity of beta-sheet structures in SOD1 (48%) especially in regions varying from 83–85, 92–97, and 141–145 (aggregation triggering segments [62]) comparaed to that of WT (41%). These regions were confined to show greater intensity in the formation of beta-sheets that was earlier found to have coiled structures in WT. Moreover, the results exist in agreement with the earlier reports indicating that the A4V mutation tends to increase the propensity of beta-sheets in SOD1 [58]. Contrastingly, the regions that established an increased propensity of beta-sheets in A4V mutant became significantly reduced, when S substitutes C111, thus showing an overall reduction in beta-sheet content (43%). Therefore, the decrease in the propensity of beta-sheets in the aggregation triggering segments (141–145), presumably supported the release of protein aggregation in SOD1 protein. Further, the propensity of coil structures in WT SOD1 (55%) was found to reduce upon point mutation (A4V) in SOD1 with a decrease of 4%. Whereas, the enhancement in the propensity of coil structures in A4V_C111S mutant (54%) were seen as compared to that of A4V mutant. On the whole, the increased propensity of beta-sheet in A4V mutant got altered towards helix and coil structures, when S substitutes C111 in A4V mutant SOD1. Thus, the substantial decrease of beta-sheets in A4V_C111S mutant, particularly in aggregation triggering segments supported the experimental findings, that C111S mutation renders the disease pathogenicity and aggregation in SOD1 mutants.

Free Energy Landscape on Protein Aggregation

To evaluate the impact of mutations on the sub-conformational preferences in SOD1, the free energy landscape was computed between the coordinates of RMSD and Rg of WT and the two mutants in their conformational states. The constructed free energy landscape of WT and the

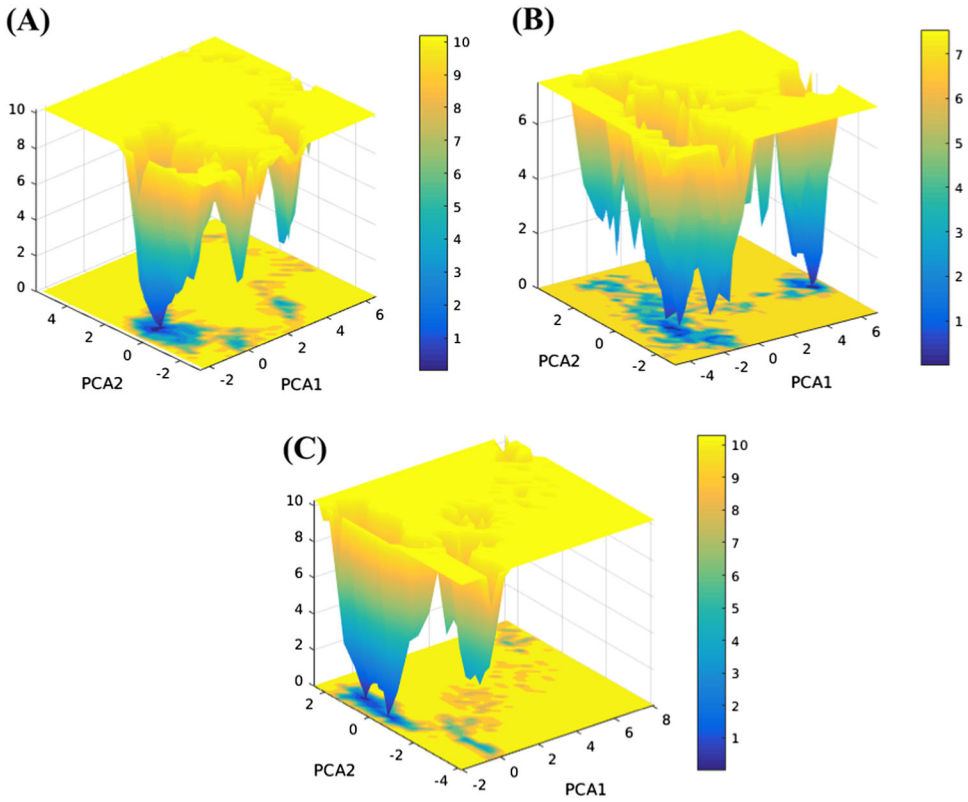

Fig. 6 3-D graphics representing the PCA1 and the PCA2 of the WT (**a**), A4V (**b**) and A4V_C111S (**c**) SOD1 proteins with the change in the free energy in terms of kcal/mol

two mutants were portrayed in Fig. 8 with the Gibbs free energy varying from 1 to 8 kcal/mol. The free energy landscape of SOD1 was found altered considerably upon A4V mutation. Moreover, the free energy landscape of WT SOD1 conformations presented a single favorable basin. The favorable basin was found located between the Rg values of 1.45 and 1.48 nm and RMSD values within 0.2 nm. The A4V mutation influences this trend and resulted in the formation of multiple favorable free energy basins at Rg values fluctuating between 1.48 and 1.52 nm and RMSD values varying between 0.2 and 0.35 nm. Therefore, the existence of A4 in WT play a prominent role in the presence of free energy basin along the RMSD and Rg that upon mutation had assessed the SOD1 to acquire multi-conformational free energy basin. Moreover, the free energy basin obtained by WT was smaller than A4V mutant conformational structures suggesting that more favored structures were adopted by WT than that of A4V mutant. Thus, the increased percentage of multiple conformers with lower energy in MT was directed towards the formation of mostly unfolded states in contrast with WT SOD1. Besides, these results hinted the irretrievable changes in the conformational structures of MT enriching the formation of toxic aggregates in SOD1. Furthermore, the results from the earlier studies have also stipulated that the aggregated proteins acquire multiple energy minima for the conformational structures that substantiate our results indirectly denoting the formation of toxic aggregates in A4V mutant SOD1 [58, 63, 64]. However, the vice versa trend was observed, when S substitutes C111 in A4V mutant SOD1. In addition, the compactness acquired by A4V mutant was found reduced upon substitution of S at C111. Interestingly, the free energy landscape of A4V_C111S exhibited a favorable basin that was confined within one particular region. The favorable basin was positioned between the Rg values of 1.45 and 1.49 nm; and the RMSD values within 0.15–0.25 nm. To be noted that the RMSD and Rg values of free energy basins in A4V_C111S mutant was relative to that of WT SOD1, but the position of free energy basin was altered upon mutation of SOD1. Therefore, the free energy landscape indicated that the substitution of C111S on A4V mutant reduced the multiple global energy minima attained by the conformers. Moreover, these results substantiate the experimental studies that the C111S mutation renders the toxic aggregates formed by the missense mutation in SOD1, which reduces the disease pathogenicity thereby, increasing the survival rate [28, 29]. Overall, the analyses from the conformational studies, secondary structure propensity, and free energy landscape untangled the mechanistic action behind the C111S mutation on aggregated A4V mutant in comparison with WT and A4V mutant SOD1. In order to authenticate, we also performed the similar studies on the other toxic SOD1 mutants (G37R, H46R, G93A, and I113T) following the same protocol. Remarkably, the

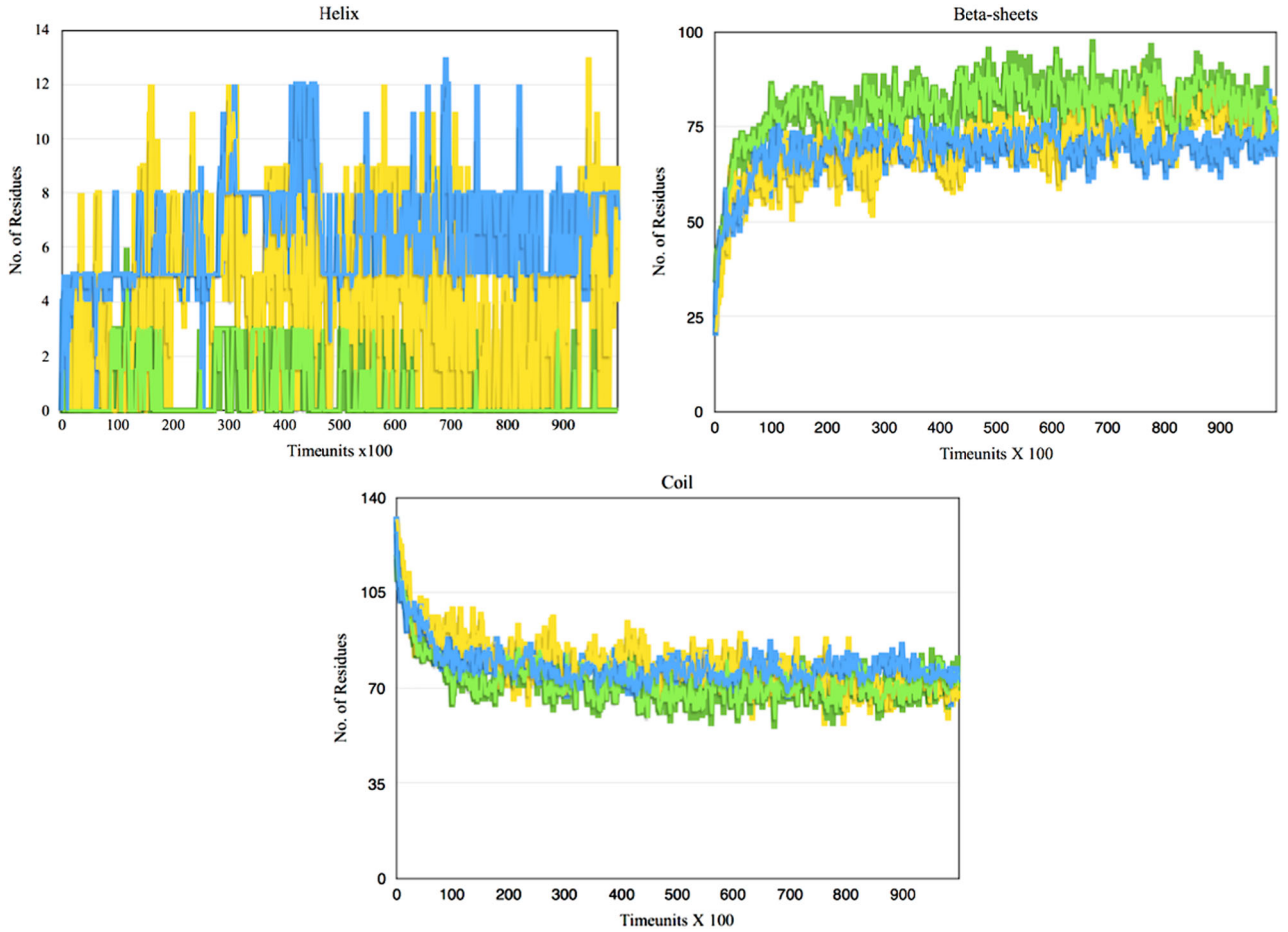

Fig. 7 The secondary structural propensity of WT (blue), A4V (green), and A4V_C111S (yellow) computed over the entire period of simulation time (color figure online)

outcomes correspond with the predictions made in our study thereby suggesting that substituting S at C111 could be beneficial not only to the devastating mutant A4V but also to other toxic SOD1 mutants affecting the mankind (Supplementary Tables and Figures).

Conclusion

The influence of the various missense mutations on SOD1 protein is still being studied and the mechanistic action behind the cause of the disease remains unknown till date. The hallmark factor of these mutations in SOD1 is the formation of insoluble toxic aggregates that increase the disease pathogenicity. In our study, the most lethal and dynamic missense mutation (A4V) on SOD1 was extensively studied, using DMD approach in comparison with WT. Thus, we reported that A4V mutation on SOD1 leads to protein aggregation and destabilization, which directs towards the ALS. In the biophysical aspects, we studied the alteration in protein structure, such as protein conformational stability, residual flexibility, compactness, free energy, and the principal motions, using distinct geometric tools for both the WT and A4V mutant conformers. Our initial analysis confirmed the effect of mutation on SOD1, which correlates with the experimental reports. To overcome the influence of A4V mutation in SOD1, we computationally studied the impact of C111S mutation in A4V mutant protein, which could render the formation of toxic aggregates and reduce disease pathogenesis as suggested by the various experimental reports. With this, we performed the DMD on A4V_C111S mutation and analyzed these similar parameters with WT and A4V mutant conformational states. Remarkably, the outcomes denoted that upon substituting S at C111 in A4V mutant, the SOD1 regained the structural stability, protein compactness, and the secondary structural propensity that was earlier found to be lost in A4V mutant. In addition to that, we analyzed the sub-conformational preferences of WT and the two mutant forms via free energy landscape. Our findings indicated that when S substitutes C111 in A4V mutant, the toxic aggregates formed by mutant conformers were reduced.

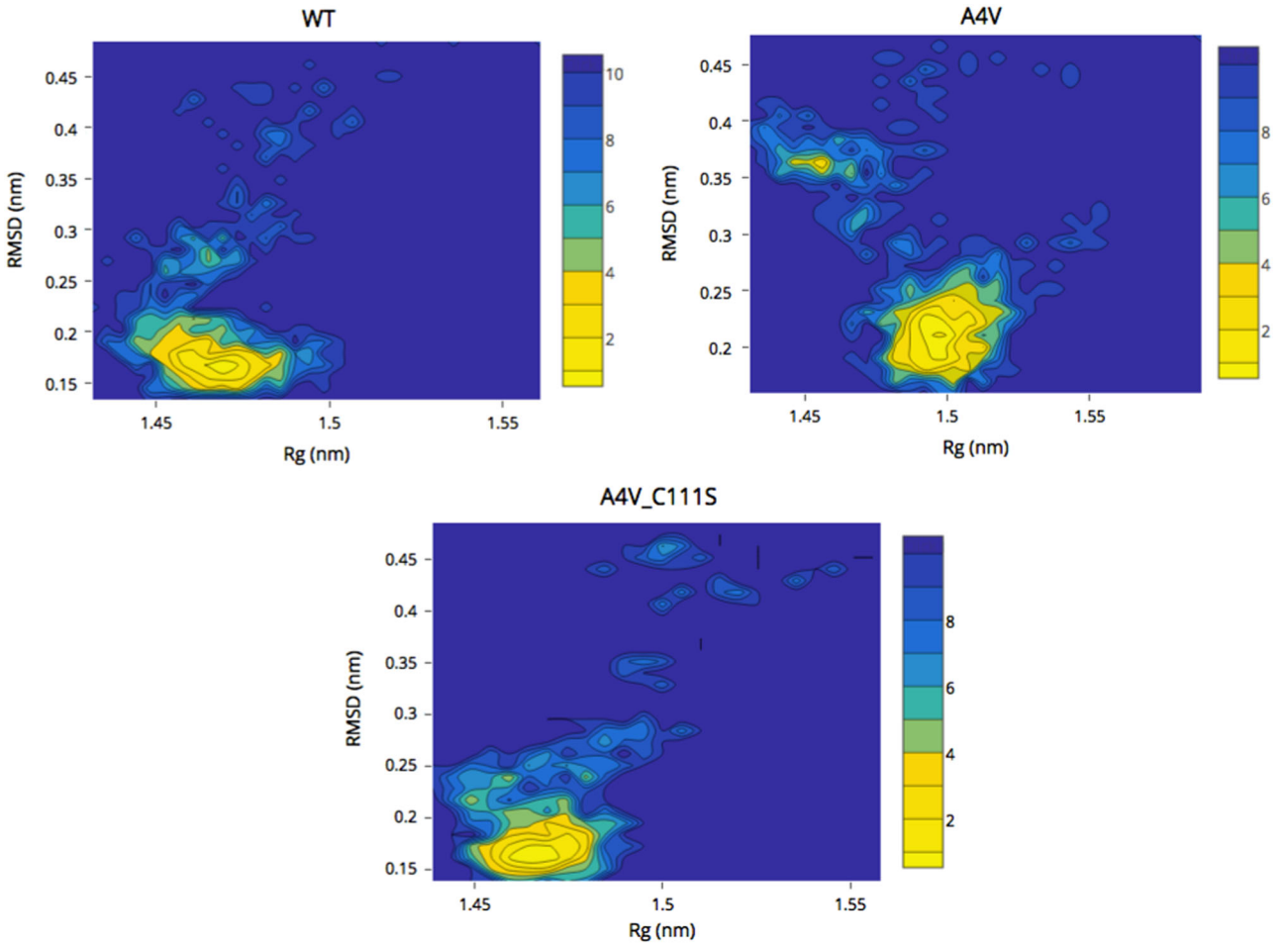

Fig. 8 Free energy landscape plotted between RMSD and Rg coordinates for WT and two SOD1 mutants. The global free energy minima formed by the WT and A4V_C111S mutant conformers were confined within one particular region over the conformational states, respectively. But the effect of A4V mutation on SOD1 altered the protein conformations urging to form multiple free energy minima, thereby indirectly representing the formation of protein aggregates

Therefore, the substituting S at C111 could be a beneficiary mutation, which could hamper the formation of toxic aggregates and thereby increase the onset survival of patients suffering from the incurable pathogenic disease causing neurodegenerative disorder ALS.

Acknowledgements The authors thank the management of VIT University for providing the facilities and encouragement to carry out this research work.

Compliance with Ethical Standards

Conflict of Interest The authors declare that they have no competing interests.

References

1. Shastry, B.S. (2003). Neurodegenerative disorders of protein aggregation. *Neurochemistry International*, *43*(1), 1–7. https://doi.org/10.1016/S0197-0186(02)00196-1.
2. Balch, W.E., Morimoto, R.I., Dillin, A., & Kelly, J.W. (2008). Adapting proteostasis for disease intervention. *Science*, *319* (5865), 916–919. https://doi.org/10.1126/science.1141448.
3. Ciryam, P., Tartaglia, G.G., Morimoto, R.I., Dobson, C.M., & Vendruscolo, M. (2013). Widespread aggregation and neurodegenerative diseases are associated with supersaturated proteins. *Cell Reports*, *5*(3), 781–790. https://doi.org/10.1016/j.celrep.2013.09.043.
4. David, D.C., Ollikainen, N., Trinidad, J.C., Cary, M.P., Burlingame, A.L., & Kenyon, C. (2010). Widespread protein aggregation as an inherent part of aging in C. elegans. *PLOS Biology*, *8* (8), e1000450. https://doi.org/10.1371/journal.pbio.1000450.
5. Rowland, L.P., & Shneider, N.A. (2001). Amyotrophic lateral sclerosis. *New England Journal of Medicine*, *344*(22), 1688–1700. https://doi.org/10.1056/NEJM200105313442207.
6. Bruijn, L.I., Houseweart, M.K., Kato, S., Anderson, K.L., Anderson, S.D., Ohama, E., & Cleveland, D.W. (1998). Aggregation and motor neuron toxicity of an ALS-linked SOD1 mutant independent from wild-type SOD1. *Science*, *281*(5384), 1851–1854. https://doi.org/10.1126/science.281.5384.1851.
7. Renton, A.E., Chiò, A., & Traynor, B.J. (2014). State of play in amyotrophic lateral sclerosis genetics. *Nature Neuroscience*, *17* (1), 17–23. https://doi.org/10.1038/nn.3584.

8. Nizzardo, M., Simone, C., Rizzo, F., Ulzi, G., Ramirez, A., Rizzuti, M., & Corti, S. (2016). Morpholino-mediated SOD1 reduction ameliorates an amyotrophic lateral sclerosis disease phenotype. *Scientific Reports*, *6*, 21301. https://doi.org/10.1038/srep21301.
9. Bucchia, M., Ramirez, A., Parente, V., Simone, C., Nizzardo, M., Magri, F., & Corti, S. (2015). Therapeutic development in amyotrophic lateral sclerosis. *Clinical Therapeutics*, *37*(3), 668–680. https://doi.org/10.1016/j.clinthera.2014.12.020.
10. Miller, R.G., Mitchell, J.D., Lyon, M., & Moore, D.H. (2003). Riluzole for amyotrophic lateral sclerosis (ALS)/motor neuron disease (MND). *Amyotrophic Lateral Sclerosis and Other Motor Neuron Disorders: Official Publication of the World Federation of Neurology, Research Group on Motor Neuron Diseases*, *4*(3), 191–206.
11. Banci, L., Bertini, I., Boca, M., Calderone, V., Cantini, F., Girotto, S., & Vieru, M. (2009). Structural and dynamic aspects related to oligomerization of apo SOD1 and its mutants. *Proceedings of the National Academy of Sciences*, *106*(17), 6980–6985. https://doi.org/10.1073/pnas.0809845106.
12. Rotunno, M.S. & Bosco, D.A. (2013). An emerging role for misfolded wild-type SOD1 in sporadic ALS pathogenesis. *Frontiers in Cellular Neuroscience*, *7*, 253. https://doi.org/10.3389/fncel.2013.00253.
13. Lasiene, J., Komine, O., Fujimori-Tonou, N., Powers, B., Endo, F., Watanabe, S., & Yamanaka, K. (2016). Neuregulin 1 confers neuroprotection in SOD1-linked amyotrophic lateral sclerosis mice via restoration of C-boutons of spinal motor neurons. *Acta Neuropathologica Communications*, *4*, 15. https://doi.org/10.1186/s40478-016-0286-7.
14. Kato, S., Sumi-Akamaru, H., Fujimura, H., Sakoda, S., Kato, M., Hirano, A., & Ohama, E. (2001). Copper chaperone for superoxide dismutase co-aggregates with superoxide dismutase 1 (SOD1) in neuronal Lewy body-like hyaline inclusions: an immunohistochemical study on familial amyotrophic lateral sclerosis with SOD1 gene mutation. *Acta Neuropathologica*, *102*(3), 233–238.
15. Proctor, E.A., Fee, L., Tao, Y., Redler, R.L., Fay, J.M., Zhang, Y., & Dokholyan, N.V. (2016). Nonnative SOD1 trimer is toxic to motor neurons in a model of amyotrophic lateral sclerosis. *Proceedings of the National Academy of Sciences*, *113*(3), 614–619. https://doi.org/10.1073/pnas.1516725113.
16. Kato, S., Takikawa, M., Nakashima, K., Hirano, A., Cleveland, D. W., Kusaka, H., & Ohama, E. (2000). New consensus research on neuropathological aspects of familial amyotrophic lateral sclerosis with superoxide dismutase 1 (SOD1) gene mutations: inclusions containing SOD1 in neurons and astrocytes. *Amyotrophic Lateral Sclerosis and Other Motor Neuron Disorders: Official Publication of the World Federation of Neurology, Research Group on Motor Neuron Diseases*, *1*(3), 163–184.
17. Julien, J.-P. (2007). ALS: astrocytes move in as deadly neighbors. *Nature Neuroscience*, *10*(5), 535–537. https://doi.org/10.1038/nn0507-535.
18. Fridovich, I. (1978). The biology of oxygen radicals. *Science*, *201*(4359), 875–880. https://doi.org/10.1126/science.210504.
19. Banci, L., Bertini, I., Cantini, F., D'Onofrio, M., & Viezzoli, M. S. (2002). Structure and dynamics of copper-free SOD: The protein before binding copper. *Protein Science: A Publication of the Protein Society*, *11*(10), 2479–2492.
20. Banci, L., Bertini, I., Boca, M., Girotto, S., Martinelli, M., Valentine, J.S., & Vieru, M. (2008). SOD1 and amyotrophic lateral sclerosis: mutations and oligomerization. *PLOS ONE*, *3*(2), e1677. https://doi.org/10.1371/journal.pone.0001677.
21. Li, H.-T., Jiao, M., Chen, J., & Liang, Y. (2010). Roles of zinc and copper in modulating the oxidative refolding of bovine copper, zinc superoxide dismutase. *Acta Biochimica et Biophysica Sinica*, *42*(3), 183–194. https://doi.org/10.1093/abbs/gmq005.
22. Valentine, J.S., Doucette, P.A., & Zittin Potter, S. (2005). Copper-zinc superoxide dismutase and amyotrophic lateral sclerosis. *Annual Review of Biochemistry*, *74*, 563–593. https://doi.org/10.1146/annurev.biochem.72.121801.161647.
23. Lo Conte, M., & Carroll, K.S. (2013). The redox biochemistry of protein sulfenylation and sulfinylation. *The Journal of Biological Chemistry*, *288*(37), 26480–26488. https://doi.org/10.1074/jbc.R113.467738.
24. Fujiwara, N., Nakano, M., Kato, S., Yoshihara, D., Ookawara, T., Eguchi, H., & Suzuki, K. (2007). Oxidative modification to cysteine sulfonic acid of Cys111 in human copper-zinc superoxide dismutase. *The Journal of Biological Chemistry*, *282*(49), 35933–35944. https://doi.org/10.1074/jbc.M702941200.
25. Wilcox, K.C., Zhou, L., Jordon, J.K., Huang, Y., Yu, Y., Redler, R.L., & Dokholyan, N.V. (2009). Modifications of superoxide dismutase (SOD1) in human erythrocytes. *The Journal of Biological Chemistry*, *284*(20), 13940–13947. https://doi.org/10.1074/jbc.M809687200.
26. Redler, R.L., Wilcox, K.C., Proctor, E.A., Fee, L., Caplow, M., & Dokholyan, N.V. (2011). Glutathionylation at Cys-111 induces dissociation of wild type and FALS mutant SOD1 dimers. *Biochemistry*, *50*(32), 7057–7066. https://doi.org/10.1021/bi200614y.
27. Cozzolino, M., Amori, I., Pesaresi, M.G., Ferri, A., Nencini, M., & Carrì, M.T. (2008). Cysteine 111 affects aggregation and cytotoxicity of mutant Cu,Zn-superoxide dismutase associated with familial amyotrophic lateral sclerosis. *Journal of Biological Chemistry*, *283*(2), 866–874. https://doi.org/10.1074/jbc.M705657200.
28. Nagano, S., Takahashi, Y., Yamamoto, K., Masutani, H., Fujiwara, N., Urushitani, M., & Araki, T. (2015). A cysteine residue affects the conformational state and neuronal toxicity of mutant SOD1 in mice: relevance to the pathogenesis of ALS. *Human Molecular Genetics*, *24*(12), 3427–3439. https://doi.org/10.1093/hmg/ddv093.
29. Roberts, B.L.T., Patel, K., Brown, H.H., & Borchelt, D.R. (2012). Role of disulfide cross-linking of mutant SOD1 in the formation of inclusion-body-like structures. *PLOS ONE*, *7*(10), e47838. https://doi.org/10.1371/journal.pone.0047838.
30. Fay, J.M., Zhu, C., Proctor, E.A., Tao, Y., Cui, W., Ke, H., & Dokholyan, N.V. (2016). A phosphomimetic mutation stabilizes SOD1 and rescues cell viability in the context of an ALS-associated mutation. *Structure*, *24*(11), 1898–1906. https://doi.org/10.1016/j.str.2016.08.011.
31. Yim, H.-S Kang, J.-H Chock, P.B., Stadtman, E.R., & Yim, M.B. (1997). A familial amyotrophic lateral sclerosis-associated A4V Cu,Zn-superoxide dismutase mutant has a lower Km for hydrogen peroxide correlation between clinical severity and the Km value. *Journal of Biological Chemistry*, *272*(14), 8861–8863. https://doi.org/10.1074/jbc.272.14.8861.
32. Wright, G.S.A., Antonyuk, S.V., Kershaw, N.M., Strange, R.W., & Samar Hasnain, S. (2013). Ligand binding and aggregation of pathogenic SOD1. *Nature Communications*, *4*, 1758. https://doi.org/10.1038/ncomms2750.
33. Schmidlin, T., Kennedy, B.K., & Daggett, V. (2009). Structural changes to monomeric CuZn superoxide dismutase caused by the familial amyotrophic lateral sclerosis-associated mutation A4V. *Biophysical Journal*, *97*(6), 1709–1718. https://doi.org/10.1016/j.bpj.2009.06.043.
34. Carballo-Pacheco, M., & Strodel, B. (2016). Advances in the simulation of protein aggregation at the atomistic scale. *The Journal of Physical Chemistry B*, *120*(12), 2991–2999. https://doi.org/10.1021/acs.jpcb.6b00059.
35. Carballo-Pacheco, M., Ismail, A.E., & Strodel, B. (2015). Oligomer formation of toxic and functional amyloid peptides studied

with atomistic simulations. *The Journal of Physical Chemistry B*, *119*(30), 9696–9705. https://doi.org/10.1021/acs.jpcb.5b04822.
36. Riccardi, L., Nguyen, P.H., & Stock, G. (2012). Construction of the free energy landscape of peptide aggregation from molecular dynamics simulations. *Journal of Chemical Theory and Computation*, *8*(4), 1471–1479. https://doi.org/10.1021/ct200911w.
37. Kalsi, N., Gopalakrishnan, C., Rajendran, V., & Purohit, R. (2016). Biophysical aspect of phosphatidylinositol 3-kinase and role of oncogenic mutants (E542K & E545K). *Journal of Biomolecular Structure & Dynamics, 34*, 1–11. https://doi.org/10.1080/07391102.2015.1127774.
38. Kumar, A., & Purohit, R. (2012). Computational screening and molecular dynamics simulation of disease associated nsSNPs in CENP-E. *Mutation Research*, *738-739*, 28–37. https://doi.org/10.1016/j.mrfmmm.2012.08.005.
39. Rajendran, V., & Sethumadhavan, R. (2014). Drug resistance mechanism of PncA in Mycobacterium tuberculosis. *Journal of Biomolecular Structure & Dynamics*, *32*(2), 209–221. https://doi.org/10.1080/07391102.2012.759885.
40. Rajendran, V., Gopalakrishnan, C., & Purohit, R. (2016). Impact of point mutation P29S in RAC1 on tumorigenesis. *Tumour Biology: The Journal of the International Society for Oncodevelopmental Biology and Medicine*, *37*(11), 15293–15304. https://doi.org/10.1007/s13277-016-5329-y.
41. Rajendran, V., Purohit, R., & Sethumadhavan, R. (2012). In silico investigation of molecular mechanism of laminopathy caused by a point mutation (R482W) in lamin A/C protein. *Amino Acids*, *43*(2), 603–615. https://doi.org/10.1007/s00726-011-1108-7.
42. Purohit, R., Rajendran, V., & Sethumadhavan, R. (2010). Relationship between mutation of serine residue at 315th position in M. tuberculosis catalase-peroxidase enzyme and Isoniazid susceptibility: An in silico analysis. *Journal of Molecular Modeling*, *17*(4), 869–877. https://doi.org/10.1007/s00894-010-0785-6.
43. Purohit, R. (2014). Role of ELA region in auto-activation of mutant KIT receptor: a molecular dynamics simulation insight. *Journal of Biomolecular Structure & Dynamics*, *32*(7), 1033–1046. https://doi.org/10.1080/07391102.2013.803264.
44. Kumar, A., Randhawa, V., Acharya, V., Singh, K., & Kumar, S. (2016). Amino acids flanking the central core of Cu,Zn superoxide dismutase are important in retaining enzyme activity after autoclaving. *Journal of Biomolecular Structure and Dynamics*, *34*(3), 475–485. https://doi.org/10.1080/07391102.2015.1049551.
45. Berman, H.M., Westbrook, J., Feng, Z., Gilliland, G., Bhat, T.N., Weissig, H., & Bourne, P.E. (2000). The protein data bank. *Nucleic Acids Research*, *28*(1), 235–242.
46. Hess, B., Kutzner, C., van der Spoel, D., & Lindahl, E. (2008). GROMACS 4: algorithms for highly efficient, load-balanced, and scalable molecular simulation. *Journal of Chemical Theory and Computation*, *4*(3), 435–447. https://doi.org/10.1021/ct700301q.
47. Darden, T., York, D., & Pedersen, L. (1993). Particle mesh Ewald: an N·log(N) method for Ewald sums in large systems. *The Journal of Chemical Physics*, *98*(12), 10089 https://doi.org/10.1063/1.464397.
48. Shirvanyants, D., Ding, F., Tsao, D., Ramachandran, S., & Dokholyan, N.V. (2012). Discrete molecular dynamics: an efficient and versatile simulation method for fine protein characterization. *The Journal of Physical Chemistry B*, *116*(29), 8375–8382. https://doi.org/10.1021/jp2114576.
49. Ding, F., Tsao, D., Nie, H., & Dokholyan, N.V. (2008). Ab initio folding of proteins with all-atom discrete molecular dynamics. *Structure*, *16*(7), 1010–1018. https://doi.org/10.1016/j.str.2008.03.013.
50. Ding, F., Tsao, D., Nie, H., & Dokholyan, N.V. (2008). Ab initio folding of proteins with all-atom discrete molecular dynamics. *Structure*, *16*(7), 1010–1018. https://doi.org/10.1016/j.str.2008.03.013.
51. Lazaridis, T., & Karplus, M. (1999). Effective energy function for proteins in solution. *Proteins*, *35*(2), 133–152.
52. Andersen, H.C. (1980). Molecular dynamics simulations at constant pressure and/or temperature. *The Journal of Chemical Physics*, *72*(4), 2384–2393. https://doi.org/10.1063/1.439486.
53. Ding, F., Tsao, D., Nie, H., & Dokholyan, N.V. (2008). Ab initio folding of proteins with all-atom discrete molecular dynamics. *Structure*, *16*(7), 1010–1018. https://doi.org/10.1016/j.str.2008.03.013.
54. Amadei, A., Linssen, A.B., & Berendsen, H.J. (1994). Essential dynamics of proteins. *Proteins Structure Function and Bioinformatics*, *17*(4), 412–425.
55. Likić, V.A., Gooley, P.R., Speed, T.P., & Strehler, E.E. (2005). A statistical approach to the interpretation of molecular dynamics simulations of calmodulin equilibrium dynamics. *Protein Science: A Publication of the Protein Society*, *14*(12), 2955–2963. https://doi.org/10.1110/ps.051681605.
56. Khare, S.D., & Dokholyan, N.V. (2006). Common dynamical signatures of familial amyotrophic lateral sclerosis-associated structurally diverse Cu, Zn superoxide dismutase mutants. *Proceedings of the National Academy of Sciences of the United States of America*, *103*(9), 3147–3152. https://doi.org/10.1073/pnas.0511266103.
57. Schmidlin, T., Kennedy, B.K., & Daggett, V. (2009). Structural changes to monomeric CuZn superoxide dismutase caused by the familial amyotrophic lateral sclerosis-associated mutation A4V. *Biophysical Journal*, *97*(6), 1709–1718. https://doi.org/10.1016/j.bpj.2009.06.043.
58. Srinivasan, E., & Rajasekaran, R. (2016). Computational investigation of curcumin, a natural polyphenol that inhibits the destabilization and the aggregation of human SOD1 mutant (Ala4Val), *RSC Advances*, *6*(104), 102744–102753. https://doi.org/10.1039/C6RA21927F.
59. Srinivasan, E., & Rajasekaran, R. (2016). Computational simulation analysis on human SOD1 mutant (H80R) exposes the structural destabilization and the deviation of Zn binding that directs familial amyotrophic lateral sclerosis. *Journal of Biomolecular Structure & Dynamics*, *35*, 1–9. https://doi.org/10.1080/07391102.2016.1227723.
60. Ding, F., & Dokholyan, N.V. (2008). Dynamical roles of metal ions and the disulfide bond in Cu, Zn superoxide dismutase folding and aggregation. *Proceedings of the National Academy of Sciences*, *105*(50), 19696–19701. https://doi.org/10.1073/pnas.0803266105.
61. Coskuner, O., Wise-Scira, O., Perry, G., & Kitahara, T. (2013). The structures of the E22Δ mutant-type amyloid-β alloforms and the impact of E22Δ mutation on the structures of the wild-type amyloid-β Alloforms. *ACS Chemical Neuroscience*, *4*(2), 310–320. https://doi.org/10.1021/cn300149j.
62. Ivanova, M.I., Sievers, S.A., Guenther, E.L., Johnson, L.M., Winkler, D.D., Galaleldeen, A., & Eisenberg, D.S. (2014). Aggregation-triggering segments of SOD1 fibril formation support a common pathway for familial and sporadic ALS. *Proceedings of the National Academy of Sciences of the United States of America*, *111*(1), 197–201. https://doi.org/10.1073/pnas.1320786110.
63. Keerthana, S.P., & Kolandaivel, P. (2015). Structural investigation on the electrostatic loop of native and mutated SOD1 and their interaction with therapeutic compounds. *RSC Advances*, *5*(44), 34630–34644. https://doi.org/10.1039/C5RA00286A.
64. Viet, M.H., Ngo, S.T., Lam, N.S., & Li, M.S. (2011). Inhibition of aggregation of amyloid peptides by beta-sheet breaker peptides and their binding affinity. *The Journal of Physical Chemistry B*, *115*(22), 7433–7446. https://doi.org/10.1021/jp1116728.